5-2014

Embrittlement in CN3MN Grade Superaustenitic Stainless Steels

Mertcan Başkan
Middle East Technical University

L. Scott Chumbley
Iowa State University, chumbley@iastate.edu

Yunus Eren Kalay
Middle East Technical University

Embrittlement in CN3MN Grade Superaustenitic Stainless Steels

Abstract
Superaustenitic stainless steels (SSS) are widely used in extreme environments such as off-shore oil wells, chemical and food processing equipment, and seawater systems due to their excellent corrosion resistance and superior toughness. The design of the corresponding heat treatment process is crucial to create better mechanical properties. In this respect, the short-term annealing behavior of CN3MN grade SSS was investigated by a combined study of Charpy impact tests, hardness measurements, scanning and transmission electron microscopy. Specimens were heat treated at 1200 K (927 °C) for up to 16 minutes annealing time and their impact strengths and hardnesses were tested. The impact toughness was found to decrease to less than the half of the initial values while hardness stayed the same. Detailed fracture surface analyses revealed a ductile to brittle failure transition for relatively short annealing times. Brittle fracture occurred in both intergranular and transgranular modes. SEM and TEM indicated precipitation of nano-sized intermetallics, accounting for the intergranular embrittlement, along the grain boundaries with respect to annealing time. The transgranular fracture originated from linear defects seen to exist within the grains. Close observation of such defects revealed stacking-fault type imperfections, which lead to step-like cracking observed in microlength scales.

Keywords
Surfaces and Interfaces, Thin Films Nanotechnology

Disciplines
Metallurgy

Comments
This article is from *Metallurgical and Materials Transactions A* 45 (2014): 2405-2411, doi: 10.1007/s11661-013-2179-8. Posted with permission.

Embrittlement in CN3MN Grade Superaustenitic Stainless Steels

MERTCAN BAŞKAN, SCOTT L. CHUMBLEY, and YUNUS EREN KALAY

Superaustenitic stainless steels (SSS) are widely used in extreme environments such as off-shore oil wells, chemical and food processing equipment, and seawater systems due to their excellent corrosion resistance and superior toughness. The design of the corresponding heat treatment process is crucial to create better mechanical properties. In this respect, the short-term annealing behavior of CN3MN grade SSS was investigated by a combined study of Charpy impact tests, hardness measurements, scanning and transmission electron microscopy. Specimens were heat treated at 1200 K (927 °C) for up to 16 minutes annealing time and their impact strengths and hardnesses were tested. The impact toughness was found to decrease to less than the half of the initial values while hardness stayed the same. Detailed fracture surface analyses revealed a ductile to brittle failure transition for relatively short annealing times. Brittle fracture occurred in both intergranular and transgranular modes. SEM and TEM indicated precipitation of nano-sized intermetallics, accounting for the intergranular embrittlement, along the grain boundaries with respect to annealing time. The transgranular fracture originated from linear defects seen to exist within the grains. Close observation of such defects revealed stacking-fault type imperfections, which lead to step-like cracking observed in microlength scales.

DOI: 10.1007/s11661-013-2179-8

I. INTRODUCTION

AUSTENITIC stainless steels are a subclass of stainless steels containing austenite as a primary phase at room temperature due to the high amount of nickel constituent. Like other types of stainless steels, most of them are susceptible to pitting corrosion in chlorine environments. A common index known as pitting resistance equivalent number ($PREN_{30}$) is commonly used in stainless steels to give a quantitative measure of pitting corrosion resistance. The empirical formula representing $PREN_{30}$ is given as[1]:

$$PREN_{30} = pctCr + 3.3 \times (pctMo) + 30 \times (pctN). \quad [1]$$

The steels which have higher $PREN_{30}$ than 45 are generally known as superaustenitic stainless steels (SSS) and they combine high strength and toughness with excellent corrosion performance. As compared to conventional austenitic stainless steels, they are widely used in extreme environments due to their superior resistance to pitting and crevice corrosion at high temperatures and in seawater. They also have high resistance to chloride-induced corrosion and stress corrosion cracking. Off-shore oil wells, seawater handling, chemical and food processing equipment in addition to heat exchangers and piping in purification systems are the application areas of SSS.[2]

Equation [1] clearly shows that pitting resistance can be enhanced by increasing the amount of chromium and molybdenum. However, when superaustenitic steels are exposed to high temperatures, such as 823 K to 1223 K (550 °C to 950 °C), the formation of intermetallic phases is almost inevitable due to the high alloying content.[3,4] Most of the intermetallics are detrimental for both corrosion resistance and mechanical properties; therefore, they have been investigated and classified in various studies. The most common intermetallics observed in SSSs are sigma (σ), chi (χ), laves phase, nitrides (Cr_2N, CrN, and π), and some carbides like $M_{23}C_6$ and M_6C depending on the alloying elements and composition.[5–8]

Proper heat treatment is very crucial in SSSs because inadequate heat treatment is almost always followed by intermetallic formation, degrading the mechanical properties. Several studies have shown that the sigma phase is responsible for the embrittlement observed in the SSSs.[9,10] Sigma precipitates at grain boundaries, therefore, small grained-structures provide a greater opportunity for grain boundary nucleation.[11] They can also form intragranularly, but intergranular formed sigma particles have faster growth kinetics and a higher coarsening rate as opposed to intragranular ones.[12] Similar to sigma phase, chi also prefers grain boundaries and triple junctions, however, they can also be seen intragranularly. Laves phase is a secondary phase that transforms to sigma phase after long annealing times, implying that the sigma phase is the more stable of the

MERTCAN BAŞKAN, Research Assistant and YUNUS EREN KALAY, Assistant Professor, are with the Department of Metallurgical and Materials Engineering, Middle East Technical University 06800 Ankara, Turkey. Contact e-mail: ekalay@metu.edu.tr SCOTT L. CHUMBLEY, Professor, is with the Department of Materials Science and Engineering, Iowa State University, Ames, IA 50010.

Manuscript submitted September 19, 2013.
Article published online January 7, 2014

two.[2] Cr_2N has a complex precipitation process including initial cellular precipitation followed by discontinuous lamellar formation called "nitrogenous pearlite".[8]

The formation kinetics of these various types of precipitates is extremely sluggish. Phillips *et al.* showed that after annealing 1000 minutes at 1173 K (900 °C), the measured volume percent of sigma phase is less than 2 vol pct, and around 6 vol pct Laves phase. They also found that the volume percent of the precipitates was still increasing even after 2040 h annealing heat treatment at 1073 K (800 °C), which means the system had not reach equilibrium yet.[13] Muller and Scott Chumbley[4] studied the fracture mechanism of CN3MN and concluded that almost no grain boundary precipitation coverage was seen in 5 minutes heat treatment, however, it reached up to 65 pct after annealing for 60 minutes at 1105 K (872 °C), which resulted in intergranular fracture occurring in SSSs.

Although the intermetallics formed in SSSs and their affects after long-term annealing processes have been examined by various studies,[2,4,8,12,13] the subtle embrittlement after short annealing time has not been understood clearly. Moreover, because of the slow kinetics of precipitation, there may be different mechanisms for this brittleness other than the formation of secondary phases.

The main purpose of the study is to investigate possible reasons of embrittlement after relatively short annealing times at certain temperatures in CN3MN grade SSSs, which is the cast counterpart of Al-6XN. Charpy impact tests and hardness measurements were applied to samples heat treated up to 16 minutes at 1100 K (927 °C). The fracture surfaces were investigated using scanning electron microscopy (SEM). The corresponding microstructures were examined with a combined study of transmission (TEM) and SEM, electron back-scattered diffraction (EBSD), and energy dispersive spectroscopy (EDS).

II. EXPERIMENTAL PROCEDURE

Test specimens were produced in collaboration with Steel Founders' Society of America (SFSA) foundries in the form of 3 × 3 × 35 cm keel bars. These keel bars were subjected to solution heat treatment at 1477 K (1204 °C) and water quenched to obtain a fully homogeneous austenitic structure. Half-size Charpy blanks were machined from keel bars 5 × 5 × 55 mm in size according to the ASTM E-23 standard and notched by electrical discharge machining (EDM). The Charpy impact samples were encapsulated in a quartz tube and the heat treatment was conducted in a vertical tube furnace for times ranging from 0 to 16 minutes at 1200 K (927 °C) as shown in Table I. After the annealing heat treatment, the specimens were water quenched.

Table I. The Codes and Annealing Times for Specimens Heat Treated at 1200 K (927 °C)

Samples	S0	S0.5	S1	S2	S4	S8	S16
Annealing times	0 min	30 s	1 min	2 min	4 min	8 min	16 min

Charpy impact and hardness tests were applied to all heat-treated samples using a Tinius Olsen Charpy Impact Tester and EmcoTest M4U-025 Hardness Tester at room temperatures. Hardness tests were conducted in the Rockwell B Scale and impact energies were measured in Joules. The microstructure and fracture surfaces were examined using an FEI Nova NanoSEM 430 model field emission scanning electron microscope equipped with EDS and EBSD attachment. Marble's reagent was used in metallographic specimen preparation. Specimens for EBSD were prepared using Struers LectroPol-5 Electropolisher with 5 pct perchloric acid and 95% ethanol solution at 30 V for 10 seconds. TEM analyses were conducted by a JEOL JEM2100F field emission gun scanning/transmission electron microscope. Samples for electron microscopy were electropolished with a solution of 33 pct nitric acid and 67 pct methanol solution at 238 K (−35 °C).

III. RESULTS AND DISCUSSION

The mechanical behavior of CN3MN grade SSS was initially investigated by means of hardness and Charpy impact tests for different annealing times at 1200 K (927 °C). Figure 1 shows superimposed the hardness and impact energy data. Upon annealing, hardness results nearly stay the same at approximately 80 HRB, whereas there is a severe drop in impact energy as the annealing time increases. The decrease in the impact toughness starts at very early times of annealing and it quickly drops to one-half of the as-solutionized sample, as early as 16 minutes of annealing. The grain size analysis by standard linear intercept method shows that the grain sizes of the S0 and S16 are 1048 ± 518 μm and 949 ± 305 μm, respectively. The relatively high standard deviation results because of the elongated morphology of the non equi-axed morphology of the individual grains. The results show that the average grain size stays almost constant during short-term annealing indicating that the decrease in the impact toughness is independent of the grain size.

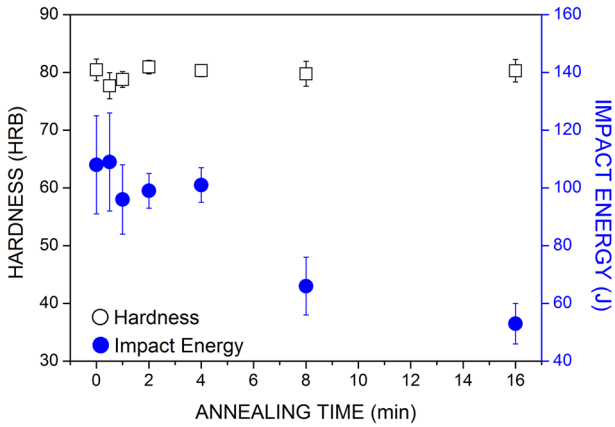

Fig. 1—The results of hardness and Charpy impacts tests after various annealing experiments.

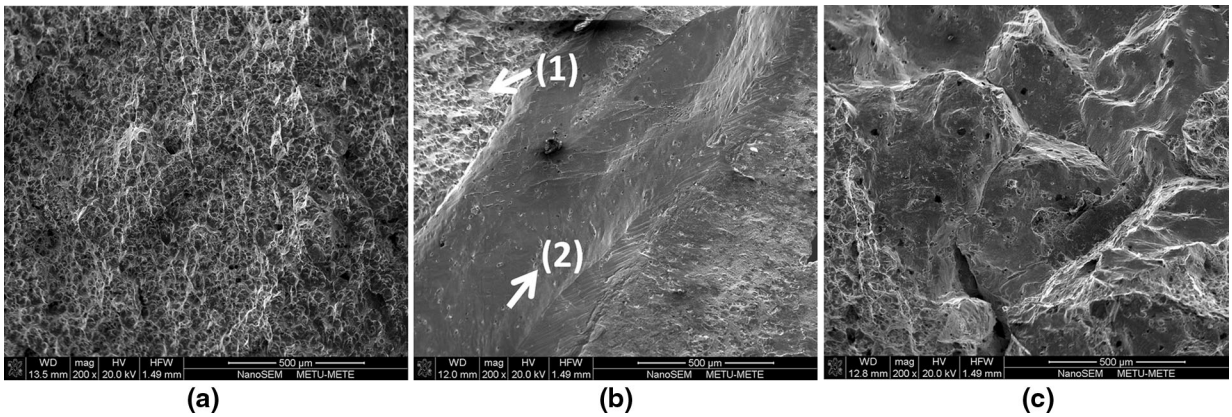

Fig. 2—Fracture surfaces of (*a*) 0 min (*b*) 4 min (*c*) 16 min annealed samples. Arrow (1) and (2) shows the dimples and the dull areas, respectively indicating a mix-mode of ductile and brittle fractures.

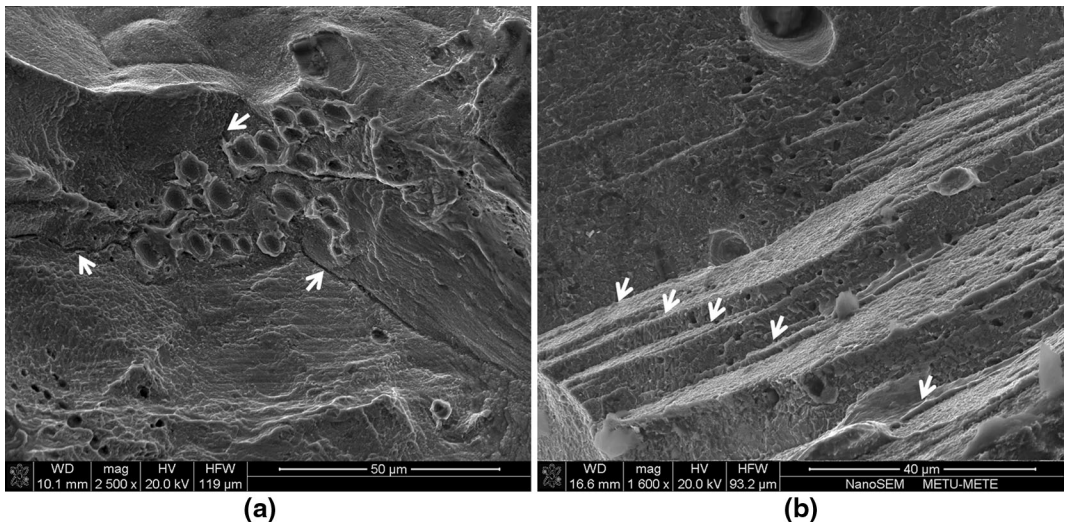

Fig. 3—The intergranular (*a*) and transgranular (*b*) brittle fracture mechanisms observed on CN3MN S16.

S0, S4, and S16 specimens were chosen for a complete failure analysis to reveal the underlying reasons for the unexpected drop in impact energy with respect to annealing times. Figure 2 shows the fracture surfaces of Charpy impact test specimens examined using SEM. The as-solution heat-treated specimen (S0) exhibited a complete ductile fracture whereas the 16 minutes-annealed specimen (S16) displayed almost a complete brittle fracture behavior. The 4 minutes-annealed specimen (S4), on the other hand, contains the characteristics of both brittle and ductile type fractures. The surface areas containing the typical features of ductile and brittle fractures are indicated by the arrows in Figure 2(b).

Brittle fracture is usually considered to arise in intergranular and transgranular modes. Intergranular brittle fracture usually occurs on the grain boundaries when a brittle phase forms a network on grain boundaries. Intermetallic formation is seen as the primary reason for intergranular fracture. Transgranular fracture, on the other hand, does not follow the grain boundary paths. Instead, they follow some crystallographic planes known as cleavage planes. Detailed fracture surface analysis of S16 specimens indicates evidence of both intergranular and transgranular brittle fractures. In Figure 3(a), cracks follow the grain boundaries and the primary crack splits into two other cracks at the triple junction, where the three grain boundaries meet in the polycrystalline material. This is a typical indication of intergranular fracture. In Figure 3(b) on the other hand, cracks are parallel to each other and they extend as step-like cleavage planes. This implies that the cracks preferred a definite crystallographic orientation rather than grain boundaries. Since there was no grain boundary failure involved in the fracture, the fracture type is transgranular.

As shown in Figure 4(a), as-solution heat-treated S0 specimen has no grain boundary segregation. This clearly indicates why this specimen does not experience an intergranular fracture and exhibited a complete ductile fracture behavior. However, with annealing time, several precipitates start to appear at grain boundaries as shown in Figure 4(b) for the S4 specimen. After only 16 minutes of annealing, the grain boundary is covered with precipitates as shown in Figure 4(c) for

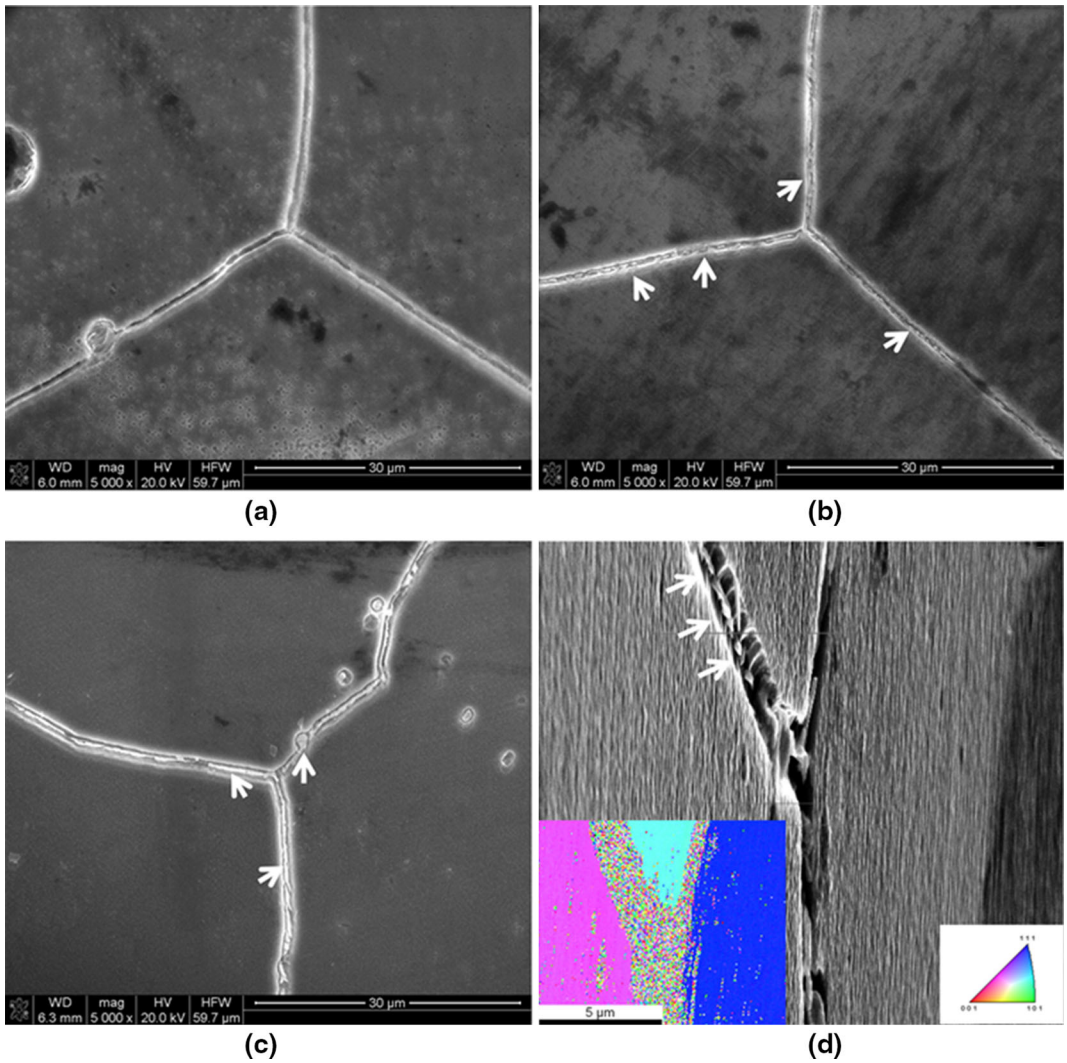

Fig. 4—Grain boundary segregation at (*a*) 0 min, (*b*) 4 min, (*c*) 16 min annealed specimens. (*d*) EBSD pattern and secondary electron image of 16 min specimen indicating the grain boundary precipitation.

the S16 specimen. These precipitates were relatively long and aligned along the grain boundaries. The EBSD analysis of a triple junction in Figure 4(d) clearly shows that the precipitation occurs preferentially at the grain boundaries. The small size of these precipitates makes it difficult to conduct a crystallographic and chemical analyses using EBSD and EDS, respectively.

While intergranular fracture is quite common after long-term annealing[1,4,13] due to precipitation it is unusual to occur so quickly after short times, and the size scale of the precipitates is too small to investigate using SEM. Additionally, the observance of transgranular fracture after short annealing times is relatively new for SSSs. Thus, both types of failures were further investigated in detail using TEM and the results are discussed in the following section.

A. *Intergranular Fracture*

Figure 5(a) shows the bright-field (BF) image of the S16 specimen showing two different grains of austenite and several precipitates formed along the grain boundary. The size and morphology of these precipitates are in good agreement with the SEM analyses. EDS analyses collected from the grains and the precipitates are shown in Table II. These analyses represent the average of five measurements. While the compositions of Grains A B are found to be very close to each other, the precipitates have a quite different chemistry as compared to the surrounding matrix, being highly enriched in Mo and Si and deficient in Mn and Fe. Cr was also found to be slightly higher within the precipitates. The overall chemistry of the precipitates could not be matched with any of the known intermetallics formed in SSS (*i.e.*, sigma, laves and chi), which may imply the presence of a new intermetallic structure.

The selected area diffraction (SAD) patterns collected from the austenite matrix along ⟨011⟩ zone axis and the precipitates are shown in left and right insets of Figure 5(a), respectively. A detailed analysis of electron diffraction was performed from the precipitates and a list of interplanar spacings calculated from three different zone axis is given in Table III. The interplanar spacing and their angular relationship could not be

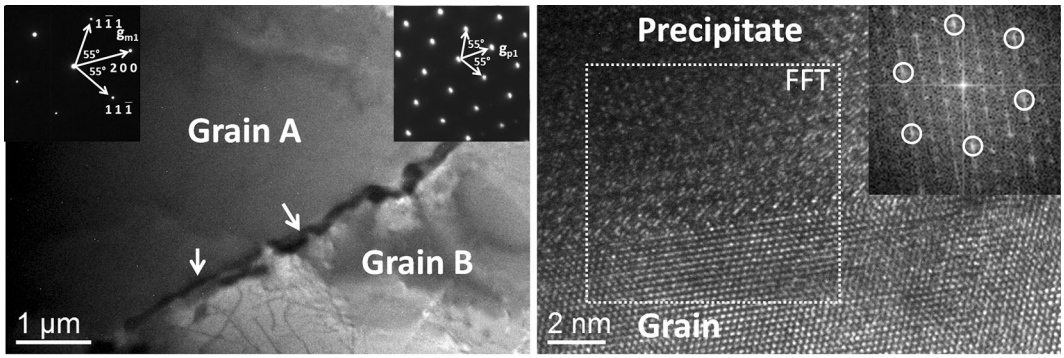

Fig. 5—TEM micrographs of (*a*) precipitates formed along the grain boundaries. Left and right insets show the SAED patterns of the matrix and precipitates, respectively. (*b*) The HRTEM image showing interface between precipitates and austenite matrix. Inset shows the FFT pattern of the square area.

Table II. The Chemical Compositions (Wt Pct) of Grain A, Grain B and Precipitates Shown in Fig. 5(a)

Area	Si	Cr	Mn	Fe	Ni	Mo
Grain A	1.0 ± 0.1	20.8 ± 0.2	1.1 ± 0.1	46.5 ± 0.3	24.0 ± 0.1	6.7 ± 0.2
Grain B	1.0 ± 0.1	20.6 ± 0.2	1.2 ± 0.0	46.4 ± 0.3	24.1 ± 0.1	6.8 ± 0.2
Precipitates	6.2 ± 0.3	22.3 ± 0.4	0.6 ± 0.1	14.3 ± 0.2	23.3 ± 0.3	33.3 ± 0.5

Table III. List of Interplanar Spacing Calculated from SAED Patters at Various Zone Axis

Interplanar Spacing (Å)
6.6
5.7
2.6
2.3
2.1
1.6

matched with any of the expected secondary phases for stainless steels as tabulated in Table IV.

One observation noted is that the diffraction data collected from the precipitates has a similar angular relationship with the fcc-austenite phase. The angular relationship of the SAD pattern collected from the precipitate in Figure 5 is exactly same as the neighboring austenite matrix along ⟨011⟩ zone axis. The interplanar spacing values, on the other hand, are different but still related to each other. The interplanar spacing between 002 planes in austenite is 1/3 of the distance of the interplanar spacing of precipitate along the same crystallographic direction. This relationship can be also seen from the high-resolution TEM (HRTEM) in Figure 5(b) collected from the same zone axis showing the interface between the austenite and the precipitate. The fast-Fourier transform calculated from the interface shows bright spots matching with austenite phase (circled in the inset) and several faint spots corresponding to the precipitate showing a similar 1/3 ratio. If a cubic structure is assumed for the precipitate regarding to the angular relationship observed in electron diffraction, the lattice parameter would become approximately 11.40 Å. This, coupled with the already mentioned angular alignment of the matrix and precipitate planes indicates a strong epitaxial relationship exists between the austenite and precipitate. An epitaxial relationship between the two phases should facilitate the rapid intermetallic precipitation decorating the grain boundaries. This agrees with the rapid growth of precipitates after only 16 minutes. The brittle nature of these precipitate eventually results in the grain boundary embrittlement observed in Figure 3(a).

B. *Transgranular Fracture*

Figure 3(b) shows transgranular cracks aligning parallel to a specific direction in a step-like manner. This is strong evidence that the transgranular cracks might originate due to crystallographic defects within the grain. Thus, the S16 specimens were examined using TEM to reveal the principal causes of the transgranular fracture mode within the crystal grains. The BF image tilted to ⟨110⟩ zone axis in Figure 6(a) shows several dislocation arrays together with narrow linear defects aligned along specific directions making the angle of 109.5 deg indicating the angle between {111} family of planes in a typical fcc-like structure. It should be noted that the {111} family of planes and ⟨110⟩ directions constitutes the slip system of fcc structure as represented by the stereographic projection in Figure 6(b). A similar type of angular relationship was observed in several studies,[17,18] however; their role in the fracture mechanism has not been thoroughly understood.

A detailed high-resolution TEM (HRTEM) analysis of the linear defects revealed sub-nanometer wide stacking-fault-like imperfections within the matrix. Figure 7(a) shows an area with such defects within the grain. Figure 7(b) is the magnified view from a single defect. A zigzag atomic distribution only 8 Å in length

Table IV. The Characteristic Second Phases Observed in Stainless Steel[14–16]

Phases	Lattice Type	Lattice Parameter (Å)	EDS Composition (Wt Pct)
Sigma (σ)	BCT	$a = 8.80$, $c = 4.54$	23.6Fe-45.7Cr-16.3Ni-12.6Mo
Laves (η)	HCP	$a = 4.744$, $c = 7.725$	25.4Fe-11.5Cr-7.4Ni-52.6Mo
Chi (χ)	BCC	$a = 8.862$–8.92	36Fe-36Ni-18Cr-4Mo 36Fe-12Cr-10Mo

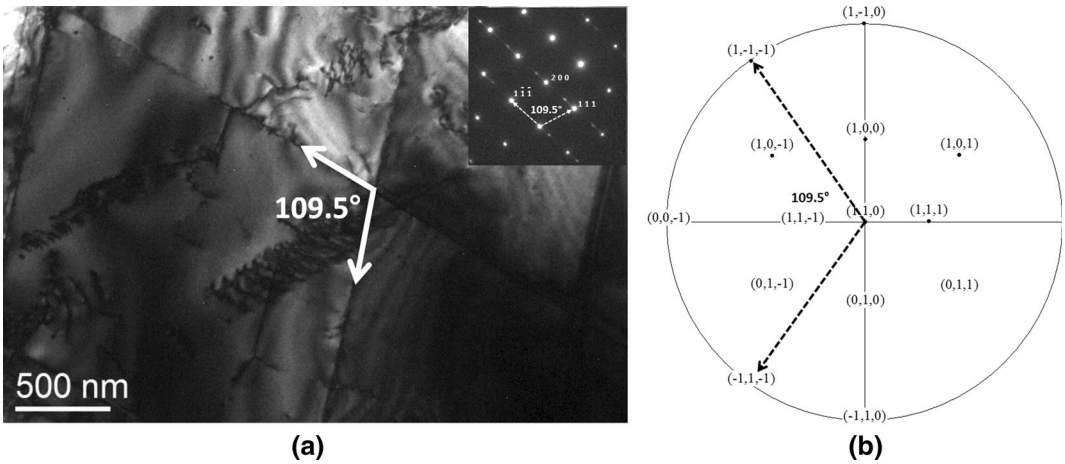

Fig. 6—(*a*) BF TEM micrographs of the matrix with dislocation and linear defects. Inset shows the SAD pattern through ⟨110⟩ zone axis. (*b*) Standard [110] stereographic projection indicating the crystallographic relationship in fcc slip system.

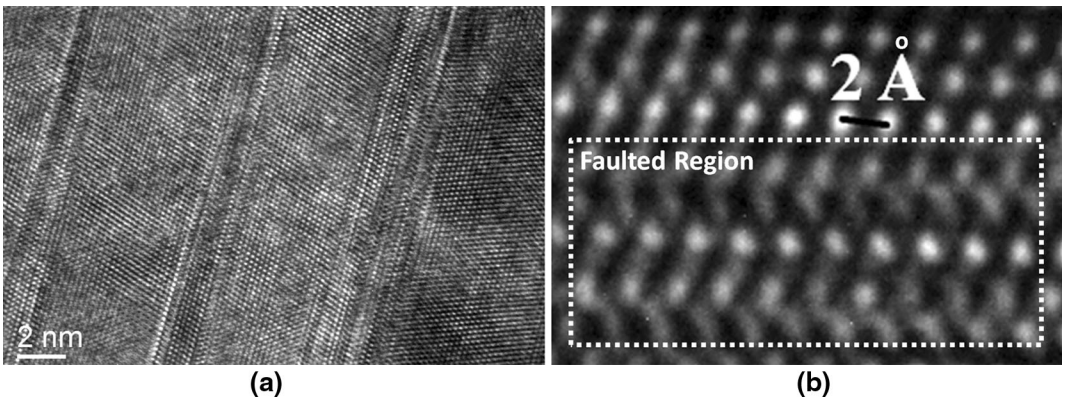

Fig. 7—HRTEM images of (*a*) several linear defects extending parallel to each other. (*b*) A magnified HRTEM view of faulted region.

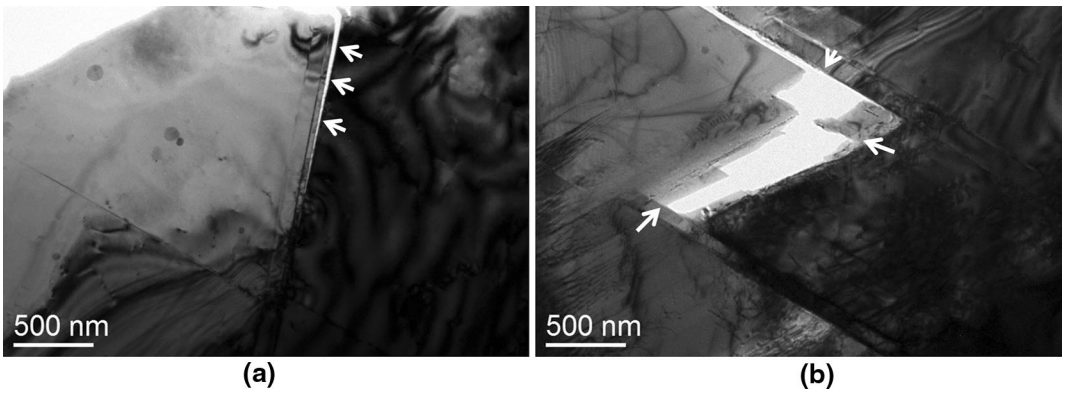

Fig. 8—BF TEM micrographs of (*a*) fracture initiated by linear defects. (*b*) Zigzag fracture pattern resembling the step-like transgranular fracture observed in S16 specimens.

can be seen in Figure 7(b). Since these defects are absent in the S0 specimen, it appears that the matrix structure itself is being strained in some manner as to produce a more brittle structure after the annealing process. One intriguing observation is that a relationship appears to exist between these linear defects and the crack pattern observed in Figure 3(b). During TEM specimen preparations cracking of the foil is almost always associated with these defects, *i.e.*, transgranular fracture of the TEM samples follow the stacking-faults observed within the grains. While the cracks definitely resulted during specimen preparation, they were only observed in brittle specimens in regions containing defects within the grains. Examples of areas with cracks associated with defects are shown in Figures 8(a) and (b) for 16 minutes specimens. Note in particular that the zigzag pattern observed in Figure 8(b) shows the tendency of transgranular fracture to generate step-like microsurfaces similar to those revealed by SEM and shown in Figure 3(b). Further analysis is required to uncover the underlying mechanism for the generation of defects after short-term annealing procedures.

IV. CONCLUSIONS

The mechanical behavior of CN3MN grade SSS was investigated after a short-term annealing process for times ranging from 0 up to 16 minutes at 1200 K (927 °C). Charpy impact tests showed a sharp decrease in impact toughness while the hardness remained almost unchanged. SEM investigations revealed the initiation of a ductile to brittle fracture mode change after 4 minutes of annealing. After 16 minutes, CN3MN grade stainless steel became completely brittle. Fracture surface analyses indicated both intergranular and transgranular cracking in annealed specimens. The intergranular fracture was initiated due to Mo- and Si-rich nanosized precipitates located at the grain boundaries. These precipitates could not be matched with any of the known second phase structures in stainless steels according to EDS and diffraction studies by using TEM. The preliminary studies have indicated an fcc-like structure with a lattice parameter of 11.40 Å. The transgranular fracture was thought to originate due to cracks nucleated at the intersection points of linear defects aligned along specific crystallographic directions. HRTEM analysis indicated these defects were similar to stacking-faults in nature. The observed cracking results in microscale step-like fracture surfaces that morphologically are in good agreement with the defect induced cracking observed within the crystal grains using SEM.

ACKNOWLEDGMENTS

This work was finacially supported by METU-BAP. The authors would like to thank to Ms. Sermin Ozlem Turhan for her valuable help in specimen preparation.

REFERENCES

1. J. Anburaj, S.S. Mohamed Nazirudeen, R. Narayanan, B. Anandavel, and A. Chandrasekar: *Mater. Sci. Eng., A*, 2012, vol. 535, pp. 99–107.
2. T. Koutsoukis, A. Redjaima, and G. Fourlaris: *Solid State Phenom.*, 2011, vols. 172–174 (2011), pp. 493–98.
3. A. Hoseini Asli and A. Zarei-Hanzaki: *J. Mater. Sci. Technol.*, 2009, vol. 25, pp. 603–606.
4. C. Muller and L. Scott Chumbley: *J. Mater. Eng. Perform.*, 2010, vol. 19 (5), pp. 714–20.
5. E.O. Hall and S.H. Algie: *Metall. Rev.*, 1966, vol. 11, pp. 61–88.
6. J.S. Kasper: *Acta Metall. Mater.*, 1954, vol. 2, pp. 456–61.
7. J.O. Nilsson and P. Liu: *Mater. Sci. Technol.*, 1991, vol. 7, pp. 853–62.
8. F. Shi, L. Wang, W. Cui, and C. Liu: *J. Iron. Steel Res. Int.*, 2002, vol. 15 (6), pp. 72–77.
9. T.H. Chen, K.L. Weng, and J.R. Yang: *Mater. Sci. Eng., A*, 2002, vol. 338, pp. 259–70.
10. J.O. Nilsson, P. Kangas, T. Karlsson, and A. Wilson: *Metall. Mater. Trans. A*, 2000, vol. 31A, pp. 35–45.
11. Y.S. Sato and H. Kokawa: *Scripta Mater.*, 1999, vol. 40, pp. 659–63.
12. D.M.E. Villanueva, F.C.P Junior, R.L. Plaut, and A.F. Padilha: *Mater. Sci. Technol.*, 2006, vol. 22, pp. 1098–1104.
13. N.S.L. Phillips and L.S. Chumbley: *J. Mater. Eng. Perform.*, 2009, vol. 18 (9), pp. 1285–93.
14. S. Heino: *Metall. Mater. Trans. A*, 2000, vol. 31A, pp. 1893–2904.
15. T.-H. Lee, S.-J. Kim, and Y.-C. Jung: *Metall. Mater. Trans. A.*, 2000, vol. 31A, pp. 1713–23.
16. Y.J. Kim, O. Ugurlu, C. Jiang, B. Gleeson, and L.S. Chumbley: *Metall. Mater. Trans. A*, 2007, vol. 38A, pp. 203–11.
17. T.H. Lee, C.S. Oh, S.J. Kim, and S. Takaki: *Acta Metall. Mater.*, 2007, vol. 55, pp. 3649–62.
18. V. Tsakiris and D.V. Edmonds: *Mater. Sci. Eng., A*, 1999, vols. 273–275, pp. 430–36.